

Confined active matter in external fields

Vaseem A. Shaik,¹ Zhiwei Peng,² John F. Brady,² and Gwynn J. Elfring^{1,*}

¹*Department of Mechanical Engineering, Institute of Applied Mathematics,
University of British Columbia, Vancouver, BC, V6T 1Z4, Canada*

²*Division of Chemistry and Chemical Engineering, California Institute of Technology,
Pasadena, California 91125, USA*

(Dated: August 23, 2022)

We analyze a dilute suspension of active particles confined between walls and subjected to fields that can modulate particle speed as well as orientation. Generally, the particle distribution is different in the bulk compared to near the walls. In the bulk, particles tend to accumulate in the regions of low speed, but in the presence of an orienting field, particles rotate to align with the field and accumulate downstream in the field direction. At the walls, particles tend to accumulate pointing into the walls and thereby exert pressure on walls. But the presence of strong orienting fields can cause the particles to reorient away from the walls, and hence shows a possible mechanism for preventing contamination of surfaces. The pressure at the walls depends on the wall separation and the field strengths. This work demonstrates how multiple fields with different functionalities can be used to control active matter under confinement.

I. INTRODUCTION

Active matter refers to a suspension of active particles that convert stored energy to directed motion [1]. Examples include a school of fish, a flock of birds and a suspension of microorganisms. Our focus here is on active matter systems where the active particles are micron sized and hence the inertia of the particles and the induced flow is negligible. Such active matter systems exhibit rich phenomena due to the self-propelling constituents, including collective motion [2], active turbulence [3] and motility-induced phase separation [4].

The dynamics of active particles depend on characteristics such as their speed [5–9], orientation [10] and diffusivity [11], and thus a degree of control over active matter can be exerted through modulation of these properties. By subjecting active particles to external fields like magnetic fields or gravitational fields or even gradients in heat, light or fluid viscosity, active particles have been shown to perform *taxis* either by rotating to align with the external field or speeding up (or slowing down) in the field, or both. An example is *Chlamydomonas nivalis* which reorients to preferentially swim against gravity due to bottomheaviness [12]. More impressively, one can ‘paint’ with the bacterium *E. coli* by exposing the bacterial suspension to the light gradients [13] as the bacterium changes its speed in response to light. More sophisticated control of synthetic active matter has recently been demonstrated by employing external magnetic fields and discrete-time feedback loops to tune the rotational diffusivity of active colloids [11]. It is in this vein, namely controlling the dynamics of active matter, that we develop theory for confined active particles subject to fields that can modulate particle speed as well as orientation.

Several researchers have analyzed the dynamics of active particles with spatially varying speeds [4, 14–18]. When the spatial variation is slow and restricted to 1D, the number density n and the swim speed U are shown to be inversely proportional, $nU = \text{constant}$ [14]. This relation means that particles accumulate in the regions of low speed and has been shown to apply to active matter under abrupt speed changes provided that (thermal or biological) fluctuations are relatively weak [18].

Active particles also tend to accumulate at confining boundaries due to their directional persistence [19], and exert a force (or pressure) on these confining boundaries. This pressure, in the absence of any external field, is a sum of the bulk osmotic pressure and the swim pressure [20], which is the unique pressure required to confine active particles [21]. If an orienting field is also present then the particles rotate to align with the field, net polar order develops and boundary accumulation is modified [19]. Net polar order gives rise to a net average swim force and the wall pressure in this case is a sum of the swim pressure and the effective body force due to reorientation that acts on particles [19]. It has also been shown that in a bipolar orienting field, particles rotate to align along as well as against the field. This results in zero polar order but net nematic order. In such fields, the swim stress was shown to be tensorial and hence, the wall pressure is the wall normal component of the swim stress [22].

While particle speed and orientation can both be controlled by external fields [21], theory has not yet been developed for confined active matter subjected to external fields that modulate both. Specifically, the scaling law satisfied by

* gelfring@mech.ubc.ca

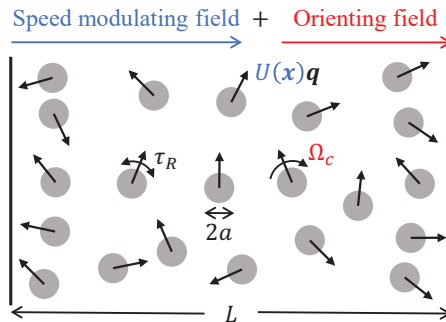


FIG. 1: A dilute suspension of spherical active particles of radius a confined between two walls that are separated by a distance L . The particles are subjected to a field that modulates their speed spatially $\mathbf{U} = U(\mathbf{x})\mathbf{q}$ and also to a field that rotates them at a rate $|\Omega_c|$. Additionally, the particles also rotate at a rate $1/\tau_R = D_R$ due to an internal reorientation mechanism.

the number density is not known, and thus previous experimental work compared results with the $nU = \text{constant}$ scaling law [23]. The theory developed in previous work for the confined active matter in the presence of a orienting field was valid for wall separations much larger the run length, which is the distance an active particle travels before reorienting due to the rotary Brownian motion [19]. Here we derive theory for active matter subjected to the two aforementioned fields, valid in the relevant limit of weak translational Brownian motion (or high activity [24]) and for all wall separations relative to the run length. We solve for the number density and wall pressure, as well as probe the theory and underlying physics that impact wall accumulation.

II. CONFINED ACTIVE PARTICLES

A. Active Brownian particles

We consider a dilute suspension of active particles confined between two infinite plane walls that are separated by a distance L . See Fig. 1 for the schematic. The particles are subjected to an external field that modulates the particles' speed spatially $\mathbf{U} = U(\mathbf{x})\mathbf{q}$, where the unit vector \mathbf{q} is the particle orientation. This can be achieved by imposing light on photo-sensitive bacteria or synthetic robots or even by spatially varying the 'fuel' that bacteria consume. The particles are also subject to an external field that leads to reorientation to align with the field direction $\hat{\mathbf{H}}$. This reorientation can be caused by imposing magnetic or gravitational fields on the magnetotactic or bottom heavy bacteria, respectively, or even by spatially varying the background fluid viscosity [25, 26]. The rate of reorientation is quantified by a characteristic angular velocity $\boldsymbol{\Omega} = \Omega_c(\mathbf{q} \times \hat{\mathbf{H}})$, that is determined from the balance between torque caused by the field (which may be hydrodynamic or external depending on the particular mechanism driving reorientation) and rotational drag. For simplicity and with no lack of generality we assume the characteristic rate $\Omega_c > 0$.

The particles are subject to fluctuations that lead to translational and rotational diffusion with diffusivities, D_T and D_R , respectively. The fluctuations may be thermal or biological in origin but regardless of the origin we consider the diffusivities to be constant and independent of the imposed background fields. Importantly, the particles in our model do not interact with one another, hydrodynamically or otherwise. This simple model of active particles is called the active Brownian particle (ABP) model and it has been used widely to understand various phenomena without any hydrodynamic interactions [27].

B. Kinetic theory

We use a kinetic theory approach developed by Saintillan and Shelley [28] to describe confined active matter in external fields. In this approach, the probability of finding a particle in the vicinity of position \mathbf{x} , and orientation \mathbf{q} at time t , $P(\mathbf{x}, \mathbf{q}, t) d\mathbf{x}d\mathbf{q}$, is governed by the Smoluchowski equation

$$\frac{\partial P}{\partial t} + \nabla \cdot \mathbf{j}_T + \nabla_R \cdot \mathbf{j}_R = 0, \quad (1)$$

where $\nabla_R = \mathbf{q} \times \partial/\partial \mathbf{q}$ and the translational and rotational fluxes are $\mathbf{j}_T = \mathbf{U}P - D_T \nabla P$ and $\mathbf{j}_R = \boldsymbol{\Omega}P - D_R \nabla_R P$, respectively. The particles are prevented from entering the walls by enforcing zero translational flux normal to the wall $\mathbf{n} \cdot \mathbf{j}_T|_{\text{wall}} = 0$, where \mathbf{n} is the unit vector normal to the wall. Also, the total number of particles is conserved by requiring that $\int \int P d\mathbf{q} d\mathbf{x} = 1$.

To capture the essential physics, we focus on the orientational moments of the probability density $P(\mathbf{x}, \mathbf{q}, t)$. The first few moments are the number density $n = \int P d\mathbf{q}$, the polar order $\mathbf{m} = \int P \mathbf{q} d\mathbf{q}$, and the nematic order $\mathbf{Q} = \int P (\mathbf{q}\mathbf{q} - \frac{1}{d}\mathbf{I}) d\mathbf{q}$, where d is the dimensionality of the problem. These moments emerge naturally expanding the probability density in terms of the irreducible tensors of the orientation \mathbf{q} , $P(\mathbf{x}, \mathbf{q}, t) = n + \mathbf{m} \cdot \mathbf{q} + \mathbf{Q} : \overline{\mathbf{q}\mathbf{q}} + O(\overline{\mathbf{q}\mathbf{q}\mathbf{q}})$, where the overbracket denotes the irreducible part of a tensor [29]. Equations governing these moments can be derived by projecting (1) onto the basis of these irreducible tensors. Hence, n and \mathbf{m} satisfy

$$\frac{\partial n}{\partial t} + \nabla \cdot \mathbf{j}_n = 0, \quad (2)$$

$$\frac{\partial \mathbf{m}}{\partial t} + \nabla \cdot \mathbf{j}_m + \Omega_c \hat{\mathbf{H}} \cdot \mathbf{Q} - \Omega_c n \hat{\mathbf{H}} \left(1 - \frac{1}{d}\right) + D_R (d-1) \mathbf{m} = \mathbf{0}, \quad (3)$$

where,

$$\mathbf{j}_n = \int \mathbf{j}_T d\mathbf{q} = U(\mathbf{x}) \mathbf{m} - D_T \nabla n, \quad (4)$$

$$\mathbf{j}_m = \int \mathbf{j}_T \mathbf{q} d\mathbf{q} = U(\mathbf{x}) \mathbf{Q} + \frac{nU(\mathbf{x})}{d} \mathbf{I} - D_T \nabla \mathbf{m}. \quad (5)$$

Similarly, moments of the no-flux condition at the walls $\mathbf{n} \cdot \mathbf{j}_T|_{\text{wall}} = 0$ yields $\mathbf{n} \cdot \mathbf{j}_n|_{\text{wall}} = 0$, $\mathbf{n} \cdot \mathbf{j}_m|_{\text{wall}} = 0$, for the first two moments. Finally, the integral constraint $\int \int P d\mathbf{q} d\mathbf{x} = 1$ implies $\int n d\mathbf{x} = 1$.

C. Analysis

We begin first by examining the relevant physical scales in the problem. There are two time scales: the reorientation time, $\tau_R = 1/D_R$, due to rotary Brownian motion or some internal biological mechanism, and the time that the field takes to reorient the particle $1/\Omega_c$. There are also three length scales: the microscopic length $h = \sqrt{D_T \tau_R}$, the run length $\ell = U_0 \tau_R$, and the channel width L , where U_0 is the self-propulsion speed in the absence of fields. We use the intrinsic reorientation time τ_R , the run length ℓ , and the speed in the absence of fields U_0 to non-dimensionalize the variables. The governing equations are ultimately characterized by three non-dimensional numbers: the Péclet number $\text{Pe} = U_0 \ell / D_T$ measuring the ratio of the self-advective (i.e., swimming) to the diffusive transport rate of particles, and two dimensionless groups which give the relative magnitude of the effects of the external fields: the relative importance of variations in speed $\alpha_L = \Delta U / U_0$, where ΔU is the characteristic change in speed, and the relative importance of the orienting field $\chi_R = \Omega_c \tau_R$.

We simplify the analysis by focusing only on the steady state solutions and consider fields that are normal to the walls. We also consider only linear speed variations; hence, for a wall normal direction \mathbf{e}_x (or $-\mathbf{e}_x$), the speed varies only along x , $\mathbf{U} = U(x) \mathbf{q}$, where $U(x) = 1 - \alpha_L \left(\frac{x}{L} - \frac{1}{2}\right)$, and the particle rotates to align with $\hat{\mathbf{H}} = \mathbf{e}_x$. Such wall normal aligned fields mean that there is no physical mechanism to induce polar order parallel to the wall or to cause any variation in that direction. Hence $n = n(x)$, $\mathbf{m} = m_x(x) \mathbf{e}_x$, and $\mathbf{Q} = Q_{xx}(x) \mathbf{e}_x \mathbf{e}_x - \frac{Q_{xx}(x)}{(d-1)} (\mathbf{I} - \mathbf{e}_x \mathbf{e}_x)$. Nematic order must be non-zero along the wall as \mathbf{Q} is trace-free.

In general, in this problem nematic order is small ($\ll n$) everywhere except possibly at the walls and there it remains small provided that Péclet numbers are modest $\text{Pe} < 10^3$ and the effects of the external fields are not dominant $\alpha_L < 1, \chi_R < 1$. See Fig. 7 in Appendix C where we plot the nematic order Q_{xx} as a function of position for various values of Pe , α_L , and χ_R , obtained from the full numerical solution of the Smoluchowski equation. Focusing (unless otherwise specified) on this range of parameter values, we neglect the nematic order, assuming $Q_{xx} = 0$, to develop an analytical theory.

Active matter systems tend to have reasonably high Péclet numbers [24], in which case the dominant transport process depends on the vicinity from the walls. In the bulk, away from the walls, advection is dominant, but near the walls, both advection and diffusion are equally important. To capture this, we perform a singular perturbation in Pe^{-1} and solve (2), and (3) separately in the bulk and in the near wall boundary layer (BL) regions, with an appropriate matching of the resulting solutions. This perturbative analysis is valid provided the BL thickness λ^{-1} is small relative to the channel width L , $\lambda^{-1} \ll L$, in other words $\text{Pe}L \gg 1$ because $\lambda \sim \text{Pe}$.

III. RESULTS

Regardless of Pe , there cannot be any particle flux normal to the wall, not just at the wall but anywhere in the domain, $\mathbf{n} \cdot \mathbf{j}_n = j_{n,x} = 0 \forall \mathbf{x}$. To derive this, integrate (2), $\nabla \cdot \mathbf{j}_n = \frac{d}{dx} j_{n,x} = 0$ using the constraint $\mathbf{n} \cdot \mathbf{j}_n|_{\text{wall}} = j_{n,x}|_{\text{wall}} = 0$.

In the bulk, neglecting translational diffusion in the flux $\mathbf{j}_n = j_{n,x} \mathbf{e}_x = \mathbf{0}$, we get $U(x) m_x = 0$. Assuming the self-propulsion speed is never zero, we find that there is no polar order in the bulk, $m_x = 0$. This is unlike the situation in the absence of walls, where net polar order exists in the presence of an orienting field [10], causing a finite particle flux. As there cannot be any particle flux in the presence of walls at steady state, there cannot be any polar order in the bulk either. Similarly, neglecting polar order and diffusion in the bulk in (3) we obtain

$$\frac{d}{dx} (nU(x)) - \chi_R n (d-1) = 0. \quad (6)$$

The solution of this equation furnishes the number density in the bulk.

Unlike in the bulk, there tends to be polar order at the walls. Particles accumulate at the walls due to their persistent motion and on average, they are aligned into the walls simply because those aligned out of the walls swim away. However, the addition of strong enough orienting field can be used to rotate the particles away from the walls, ultimately preventing any wall accumulation. This points to a possible mechanism to prevent the contamination of surfaces.

To examine the boundary layer at the left wall, we rescale the position with the BL thickness, $\bar{x} = \lambda_l x$. We eliminate m_x from $\mathbf{j}_n = \mathbf{0}$ and (3), and evaluate the speed at the left wall U_l to obtain

$$\left(\frac{U_l}{d} + \frac{(d-1)}{Pe U_l} \right) \frac{dn}{d\bar{x}} - \frac{\lambda_l^2}{Pe^2 U_l} \frac{d^3 n}{d\bar{x}^3} - \frac{\chi_R}{\lambda_l} n \left(1 - \frac{1}{d} \right) = 0. \quad (7)$$

Balancing advection with diffusion in this equation gives the BL thickness at the left wall $\lambda_l^2 \sim Pe^2 \left(\frac{U_l^2}{d} + \frac{(d-1)}{Pe} \right)$. The BL thickness is the same at both walls in the absence of the fields, $\lambda_l^{-1} = \lambda_r^{-1} = \lambda_r^{-1}$. On the other hand, balancing the reorientation with the diffusion gives the strength of the orienting field that is required to prevent any accumulation at the left wall, $\chi_R \sim \lambda_l \frac{\lambda_l^2}{Pe^2 U_l} \sim Pe$. Similar analysis can also be carried out in the BL at the right wall.

We solve the equations in the bulk and those in the BLs and form a composite expansion. We do this calculation in a number of limits, namely: no external fields ($U = 1, \chi_R = 0$), a weak speed modulating field ($\chi_R = 0, \alpha_L \ll 1$), and also a moderate orienting field ($U = 1, \chi_R < 1$). This theory is not valid for strong orienting fields ($U = 1, \chi_R \gg 1$) as nematic order becomes large and cannot be neglected; thus, we develop an alternative theory for strong orienting fields. We validate these theories by comparing them with 2D Brownian Dynamics (BD) simulations. See Appendices A, B, respectively, for the exact theoretical expressions and the BD simulation procedure.

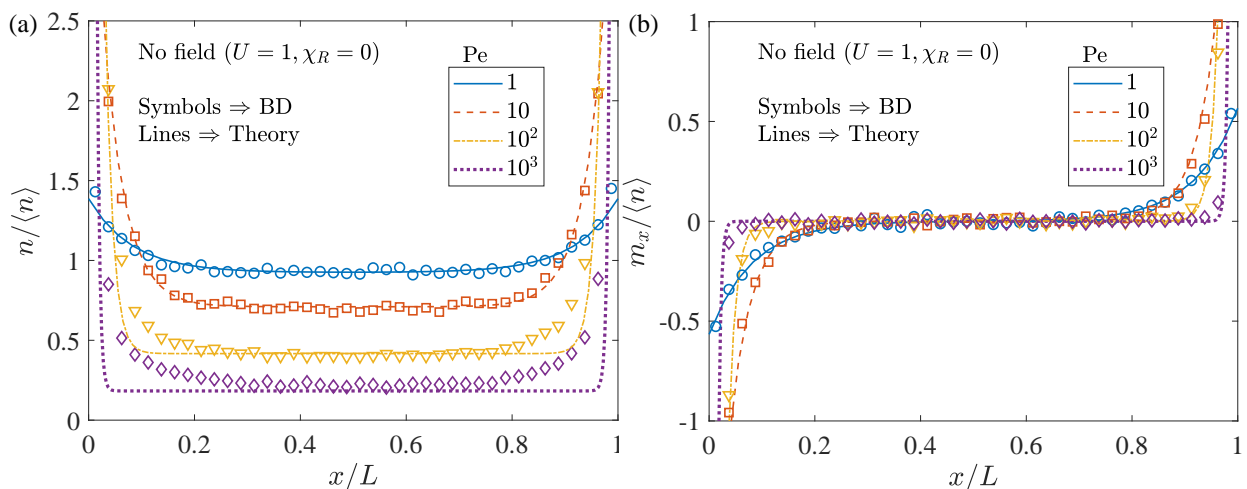


FIG. 2: In the absence of any field, the number density (a) and the polar order (b) associated with the active matter system. Here, the symbols denote the BD simulation results while the lines represent the theory (see (A6), (A7) in Appendix A). Also, the confinement region L is 10 times larger than the microscopic length h .

A. No external fields

In the absence of any external field, the self-propulsion speed $U = 1$ and the reorientation parameter $\chi_R = 0$. Then in the bulk, while the polar order is zero, the number density satisfies $nU = \text{constant}$ or simply $n = \text{constant}$ from (6) (see also Fig. 2). On the other hand, at the walls, the particles accumulate and align into the walls, hence, $m_x < 0$ at the left wall and $m_x > 0$ at the right wall. Both the number density and polar order at the wall increase while the thickness of the boundary layer decreases with increasing Pe , ($\lambda^{-1} \sim Pe^{-1}$), while the bulk concentration decreases to conserve the total number density. In this limit, the theory developed here is consistent with previous works [18, 20]. It is also in agreement with Brownian dynamics simulations at moderate Pe ; at very high Pe the theory breaks down due to the failure of the zero nematic order closure used.

When active particles collide with walls they exert a force or pressure ($\sim \text{force/area}$) on them. In the absence of external fields, the pressures exerted on the left wall and the right wall are the same, $\Pi^{LW} = n^{LW} k_B T = \Pi^{RW} = n^{RW} k_B T$ (reported here in dimensional form), where n^{LW} , n^{RW} are the number densities at the left and right walls, respectively. This wall pressure is the sum of the osmotic pressure in the bulk and the swim pressure

$$\Pi^W = \Pi^{LW} = \Pi^{RW} = n^{bulk} (k_B T + k_s T_s^0). \quad (8)$$

This formula simplifies in the high activity limit ($Pe \gg 1$) after relating the bulk concentration n^{bulk} to the average concentration $\langle n \rangle = \frac{1}{L} \int_0^L n dx$ as [20]

$$\Pi^W = \frac{\langle n \rangle (k_B T + k_s T_s^0)}{1 + \frac{2}{L\sqrt{d(d-1)}}}. \quad (9)$$

Here, the particle activity is defined as $k_s T_s^0 = Pe k_B T / d(d-1) = \zeta U_0^2 \tau_R / d(d-1)$, where ζ is the drag coefficient, k_B is the Boltzmann constant and T is the absolute temperature.

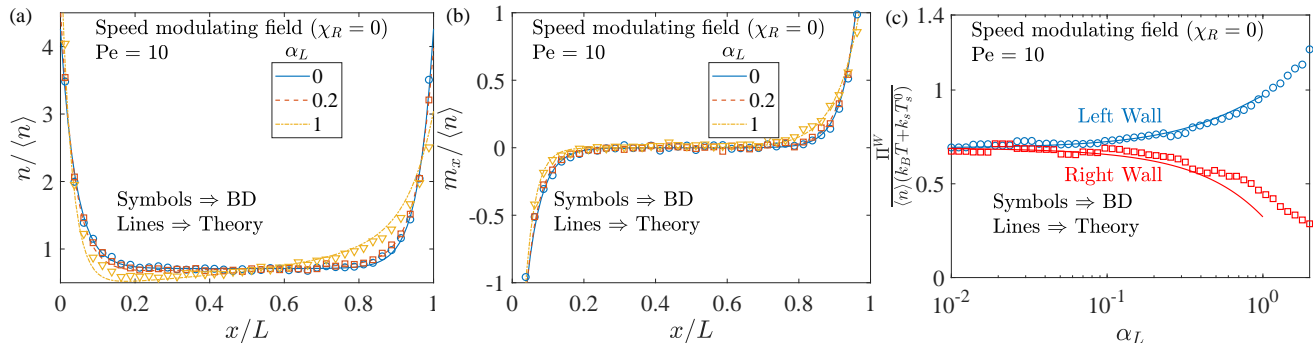


FIG. 3: The number density (a), the polar order (b), and the wall pressure (c) associated with the active matter subjected to the speed modulating field. The symbols denote the BD simulation results while the lines represent the theory. The confinement region L is 10 times larger than the microscopic length h .

B. Spatially varying speed

In the presence of a field that modulates the speed spatially, say $U = 1 - \alpha_L (\frac{x}{L} - \frac{1}{2})$ but with $\chi_R = 0$, the bulk polar order is still zero while the number density follows $nU = \text{constant}$ scaling from (6). This means that the particles in the bulk accumulate in the regions of low speed (see Fig. 3a). Additionally, the particles also accumulate at the walls. However, unlike in the bulk where the concentration decreases with increasing speed, the number density at the walls increases with higher particle speeds. Essentially this is because faster particles travel more quickly to the wall in comparison to slower ones.

The speed and hence, the accumulation at the left wall increases (and those at the right wall decrease) with an increase in the field strength α_L . These accumulated particles exert a pressure on the walls, and hence the pressure on the left and right walls correspondingly increase and decrease with increasing field strength (see Fig. 3c). In weak fields ($\alpha_L \ll 1$), the wall pressure is again the sum of the bulk osmotic pressure and the swim pressure, but evaluated

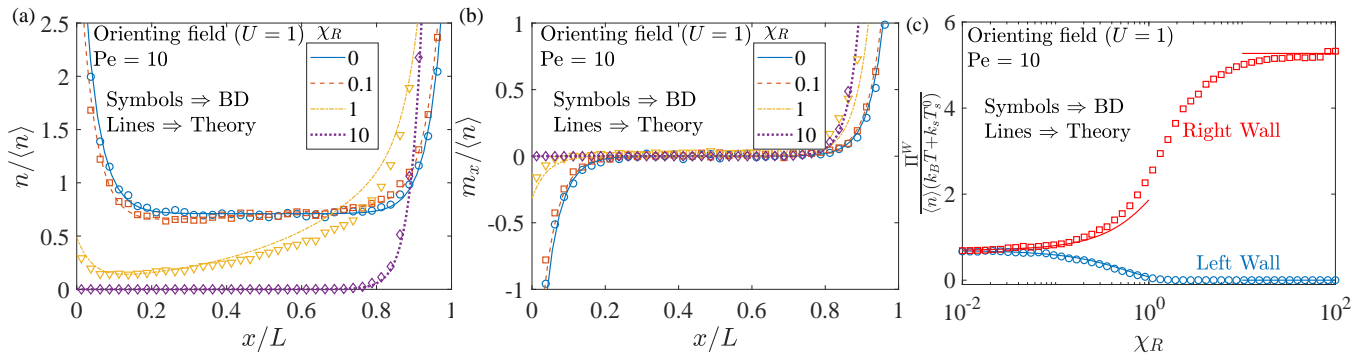


FIG. 4: The number density (a), the polar order (b), and the wall pressure (c) associated with the active matter subjected to the orienting field. The symbols denote the BD simulation results while the lines represent the theory. The confinement region L is 10 times larger than the microscopic length h .

at the wall

$$\begin{aligned}\Pi^{LW} &= n^{bulk,LW} (k_B T + k_s T_s^{LW}), \\ \Pi^{RW} &= n^{bulk,RW} (k_B T + k_s T_s^{RW}),\end{aligned}\quad (10)$$

and it simplifies at high activities ($Pe \gg 1$) to

$$\frac{\Pi^{LW}}{U_l} = \frac{\Pi^{RW}}{U_r} = \frac{\langle n \rangle (k_B T + k_s T_s^0)}{\frac{1}{\alpha_L} \ln\left(\frac{U_l}{U_r}\right) + \frac{2}{L\sqrt{d(d-1)}}}.\quad (11)$$

Here, the activity $k_s T_s$ is defined locally (in dimensional form) as $k_s T_s = \zeta U(x)^2 \tau_R / d(d-1)$ and it simplifies in the absence of field to $k_s T_s^0 = \zeta U_0^2 \tau_R / d(d-1)$. The pressure imbalance ($\Pi^{LW} \neq \Pi^{RW}$) and the resultant net force from the walls is balanced by the net swim force (that acts as a body force [19]), which can arise due to spatial variations in speed [30], or orientation bias [19] as discussed below.

C. Particles in orienting fields

In an orienting field ($U = 1, \chi_R \neq 0$), the particles rotate to align with the field for $\chi_R > 0$. Then, while the bulk polar order has to be zero to enforce the zero particle flux at steady state, the number density follows the exponential distribution from (6), $n = constant \cdot e^{(d-1)\chi_R x}$. This means the particles in bulk accumulate downstream or at right for $\chi_R > 0$ (See Fig. 4a). When $\chi_R = 0$ particles accumulate equally at both walls, but as χ_R increases, the accumulation at the right wall is increased while that at the left wall is diminished as particles are driven from left to right, the concentration and polar order thus become increasingly asymmetric as χ_R increases (see Fig. 4a and Fig. 4b).

The pressure exerted by the particles on the wall follows the same trend as the accumulation i.e., the pressure on the left and right walls, respectively, decrease and increase with increasing field strength χ_R (see Fig. 4c). Again, a simple expression for the wall pressure can be found in the limit of high activity ($Pe \gg 1$) and weak field ($\chi_R \ll 1$)

$$\frac{\Pi^{LW}}{e^{-\kappa}} = \frac{\Pi^{RW}}{e^{\kappa}} = \frac{\langle n \rangle (k_B T + k_s T_s^0)}{\frac{\sinh \kappa}{\kappa} + \frac{2}{L\sqrt{d(d-1)}} \cosh \kappa},\quad (12)$$

where $\kappa = \chi_R (d-1) L/2$.

D. Strong orienting fields

In strong orienting fields ($\chi_R \gg 1$), the nematic order at the right wall becomes important and hence cannot be neglected. See Fig. 7c in Appendix C. As the theory developed here relies on the zero nematic order closure, it is not valid in this situation. However, some physical insights can still be drawn by applying the current theory in the

strong field limit. In strong fields, for $\chi_R > 0$, we expect all the particles to align with the field, leave the left wall, and accumulate at the right wall. Hence, the left wall should be free of any particles while the accumulation at the right wall should asymptote to a value determined from the balance between the particle advection and diffusion there ($\text{Pe} n \sim \frac{dn}{dx}$). Similarly, the pressure acting on the left wall should be zero and that acting on the right wall should asymptote to a value that depends on the particle accumulation there. We next confirm these predictions by developing an alternative theory modeling the strong field limit.

Most particles in strong orienting fields ($\chi_R \gg 1$) are aligned along the field. Hence, we approximate the probability density in this case as $P(\mathbf{x}, \mathbf{q}) = n(\mathbf{x}) \delta(\mathbf{q} - \hat{\mathbf{H}})$, where δ is the Dirac delta function [31, 32]. This reduces the polar and nematic order to $m_x = n$, $Q_{xx} = n(1 - \frac{1}{d})$. Using these, we solve (2) by enforcing the constraints $\mathbf{n} \cdot \mathbf{j}_n|_{\text{wall}} = 0$ and $\frac{1}{L} \int n d\mathbf{x} = \langle n \rangle$, to ultimately find the number density that is correct at any $\text{Pe} \leq O(\chi_R)$

$$\frac{n}{\langle n \rangle} = \frac{\text{Pe}L}{(e^{\text{Pe}L} - 1)} e^{\text{Pe}x}. \quad (13)$$

However, in the limit where the earlier singular perturbation analysis is valid, $\text{Pe}L \gg 1$, the number density simplifies to

$$\frac{n}{\langle n \rangle} = \text{Pe}L e^{-\text{Pe}(L-x)}. \quad (14)$$

This equation predicts the particles are confined in a BL of thickness Pe^{-1} at the right wall (see Fig. 4a). There are no particles left in the bulk or at the left wall, hence the pressure acting on the left wall is zero. On the other hand, the pressure exerted on the right wall can be found from (14) as

$$\Pi^{LW} = 0, \quad \Pi^{RW} = \text{Pe}L \langle n \rangle k_B T = d(d-1)L \langle n \rangle k_s T_s^0. \quad (15)$$

E. Non-uniform orienting fields

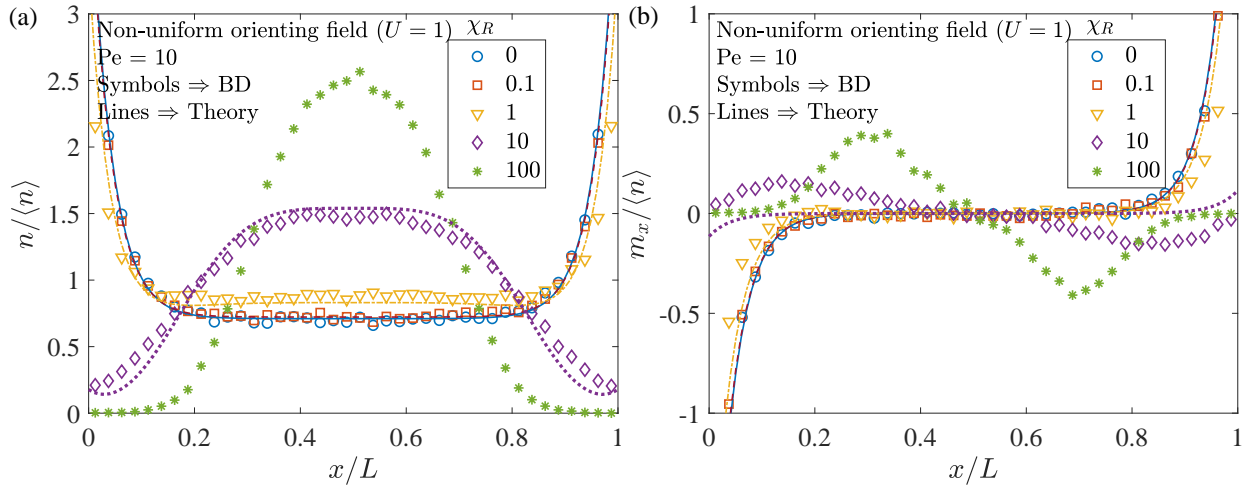


FIG. 5: The number density (a) and the polar order (b) associated with the active matter system subjected to non-uniform orienting field, $\mathbf{H} = -(2x/L - 1)^3 \hat{\mathbf{H}}$. The symbols denote the BD simulation results while the lines represent the theory. The confinement region L is 10 times larger than the microscopic length h .

In the uniform orienting fields $\mathbf{H} = \hat{\mathbf{H}}$, we discussed how the particles rotate to align with the field, ultimately leaving one wall and accumulating at the other wall in strong fields. This suggested the potential use of orienting fields in preventing accumulation at one of the walls. We can also prevent accumulation at both walls by using a non-uniform orienting field $\mathbf{H} = H(x) \hat{\mathbf{H}}$, where $H(x)$ is an odd function relative to the centerline $x = L/2$ i.e., $H(\frac{L}{2} - x) = -H(x - \frac{L}{2})$. For $H(0) > 0$, this field points away from both walls, towards the center. In such fields, the particles rotate with velocity $\boldsymbol{\Omega} = \Omega_c H(x) (\mathbf{q} \times \hat{\mathbf{H}})$ to align with the field, ultimately leaving both walls

and accumulating at the center if the field is strong enough. We demonstrate this behavior for a cubic function $H(x) = -(2x/L - 1)^3$ in Fig. 5, where we see that the particles indeed move from the wall towards the center as the field strength χ_R increases. A moderate field theory ($\chi_R \ll \text{Pe}$) for non-uniform fields can also be developed by simply replacing the constant angular velocity Ω_c or χ_R in the formulae for uniform field ((3), (6), (7)) with $\Omega_c H(x)$ or $\chi_R H(x)$. This still yields zero polar order in the bulk but a different number density $n = \text{constant} \cdot e^{\chi_R(d-1) \int H(x) dx}$.

F. Combined effects

With both speed modulating and uniform orienting fields, the physics is a combination (not necessarily a linear combination) of that for the individual fields. To illustrate this, we consider the behavior in the bulk. Here, with the speed modulating field, we know the particles accumulate in the regions of low speed. Hence, for a speed decreasing from left to right, the particles accumulate at right. On the other hand, in the orienting field, for $\chi_R < 0$, the particles rotate to align against the field and accumulate in the upstream of the field (left). Then in both fields, the particles either accumulate in the regions of low speed (right) or in the upstream of the orienting field (left) depending on the relative magnitude of the field strengths (χ_R/α_L). Also, there can be no accumulation at all ($n = \text{constant}$) if the opposing effects of the fields cancel each other. This discussion is indeed consistent with the exact expression for number density found from (6)

$$n = \frac{\text{constant}}{U^{1+(d-1)\chi_R L/\alpha_L}}, \quad (16)$$

where χ_R/α_L has to be $-1/(d-1)L$ in order for the fields to cancel each other. Also, as expected, this number density simplifies to $n = \text{constant}$ in the absence of both fields ($\chi_R, \alpha_L \rightarrow (0, 0)$) and to $nU = \text{constant}$ or $n = \text{constant} \cdot e^{(d-1)\chi_R x}$ in the presence of the speed modulating field $\chi_R \rightarrow 0$ or the orienting field $\alpha_L \rightarrow 0$, respectively.

IV. CONCLUSIONS

In summary, we analyzed confined active matter subjected to speed modulating and orienting fields. We showed that bulk polar order is always zero while the number density satisfied the usual $nU = \text{constant}$ scaling in the speed modulating fields but a different exponential distribution in orienting fields. The particles usually accumulate at the walls, but the orienting fields can be used to turn the particles away from the wall, ultimately preventing the accumulation at a wall. We also discussed the force exerted by the active matter on the confining walls and provided a concise expressions for the wall pressure.

Here we have neglected hydrodynamic interactions between the active particles and a natural next step is to include them. Hydrodynamic interaction between active particles are generally dipolar to leading order (in a dilute system) and hence determined by the \mathbf{Q} tensor field [28], which therefore cannot be neglected and more sophisticated closures (besides simple truncation) are generally used to ameliorate the hierarchy problem associated with projection of the Smoluchowski equation onto moments [32, 33].

ACKNOWLEDGEMENTS

Gwynn Elfring acknowledges the hospitality of the Division of Chemistry and Chemical Engineering at the California Institute of Technology during a sabbatical stay, supported by a UBC Killam Research Fellowship, that served as a formative period of this work and funding from the Natural Sciences and Engineering Research Council of Canada (RGPIN-2020-04850).

Appendix A: Analytical expressions for the number density and the polar order

For active matter confined between walls at $x = 0$ and L , we find the number density and polar order by solving Eqs. (2), (3) in the main text along with the constraints $\mathbf{n} \cdot \mathbf{j}_n|_{\text{wall}} = 0$ and $\mathbf{n} \cdot \mathbf{j}_m|_{\text{wall}} = \mathbf{0}$. We solve these equations asymptotically by doing a singular perturbation expansion in Pe^{-1} for $\text{Pe}L \gg 1$. Additionally, in the absence of external field, an exact solution valid at any $\text{Pe}L$ is also found. In either case, the aforementioned no-flux conditions determine solutions up to a multiplicative constant that is found using the additional constraint $\frac{1}{L} \int_0^L n dx = \langle n \rangle$.

When there is no external field ($U = 1, \chi_R = 0$), the exact solution is

$$\frac{n}{n_c} = \gamma b \left[\cosh \left(\lambda \left(x - \frac{L}{2} \right) \right) - 1 \right] + 1, \quad (\text{A1})$$

$$\frac{m_x}{n_c} = b \sinh \left(\lambda \left(x - \frac{L}{2} \right) \right), \quad (\text{A2})$$

where

$$b = \frac{\gamma}{d \left\{ 1 + \Lambda \left[\cosh \left(\frac{\lambda L}{2} \right) - 1 \right] \right\}}, \quad (\text{A3})$$

$$\lambda = \text{Pe} \sqrt{\frac{1}{d} + \frac{(d-1)}{\text{Pe}}}, \quad \Lambda = \frac{1}{1 + \frac{\text{Pe}}{d(d-1)}}, \quad \gamma = \sqrt{\frac{d}{1 + \frac{d(d-1)}{\text{Pe}}}}. \quad (\text{A4})$$

Here, n_c is the number density at the center of the confinement and can be found using the constraint $\frac{1}{L} \int_0^L n dx = \langle n \rangle$. This exact solution is consistent with the previous calculation on confined active matter [18]. The number density in (A1) rewritten as

$$\frac{n}{n_0} = 1 + \frac{\text{Pe}}{d(d-1)} \frac{\sinh(\lambda x) + \sinh(\lambda(L-x))}{\sinh(\lambda L)} \quad (\text{A5})$$

where $n_0 = \frac{n_c}{1 + \frac{\text{Pe}}{d(d-1)} \frac{1}{\cosh(\lambda L/2)}}$, is similar to that reported in Ref. [20].

The exact solution expanded in Pe^{-1} takes the form

$$\frac{n}{n^{bulk}} = 1 + \frac{\text{Pe}}{d(d-1)} \left\{ e^{-\lambda x} + e^{-\lambda(L-x)} \right\} + O(\text{Pe}^{-1}), \quad (\text{A6})$$

$$\frac{m_x}{n^{bulk}} = \frac{\lambda}{d(d-1)} \left\{ -e^{-\lambda x} + e^{-\lambda(L-x)} \right\} + O(\text{Pe}^{-1}) \quad (\text{A7})$$

where the bulk number density $n^{bulk} = n_c$. Here, the leading order terms display a linear combination of the near-wall solution [20] and the bulk solution.

In the presence of a field that modulates the self-propulsion speed (say $U = 1 - \alpha_L \left(\frac{x}{L} - \frac{1}{2} \right)$), the asymptotic solution for weak fields ($\alpha_L \ll 1$) is

$$\frac{n}{n_c} = \frac{1}{U} + \frac{\text{Pe}}{d(d-1)} \left\{ U_l e^{-\lambda_l x} + U_r e^{-\lambda_r(L-x)} \right\} + O\left(\text{Pe}^{-1}, \frac{\alpha_L}{\text{Pe}L}\right), \quad (\text{A8})$$

$$\frac{m_x}{n_c} = \frac{1}{d(d-1)} \left\{ -\lambda_l e^{-\lambda_l x} + \lambda_r e^{-\lambda_r(L-x)} \right\} + O\left(\text{Pe}^{-1}, \frac{\alpha_L}{\text{Pe}L}\right). \quad (\text{A9})$$

Here, $U_l = 1 + \frac{\alpha_L}{2}$ and $\lambda_l = \text{Pe} \sqrt{\frac{U_l^2}{d} + \frac{(d-1)}{\text{Pe}}}$ are the speed and the inverse boundary layer thickness at the left wall.

The corresponding quantities at the right wall are $U_r = 1 - \frac{\alpha_L}{2}$ and $\lambda_r = \text{Pe} \sqrt{\frac{U_r^2}{d} + \frac{(d-1)}{\text{Pe}}}$.

On the other hand, in the presence of a field that orients the particles and for field strengths $\chi_R \ll \lambda \sim \text{Pe}$, the asymptotic solution expanded in terms of $\lambda^{-1} \sim \text{Pe}^{-1}$ is

$$n = n^{(0)} + \frac{1}{\lambda} n^{(1)} + O\left(\text{Pe}^{-2}, \frac{\chi_R}{\text{Pe}^2}\right), \quad m_x = m_x^{(0)} + \frac{1}{\lambda} m_x^{(1)} + O\left(\text{Pe}^{-2}, \frac{\chi_R}{\text{Pe}^2}\right). \quad (\text{A10})$$

Here, the leading order solution is

$$\frac{n^{(0)}}{n_c^{(0)}} = e^{\chi_R(d-1)(x-L/2)} + \frac{\text{Pe}}{d(d-1)} \left\{ e^{-\chi_R(d-1)L/2} e^{-\lambda x} + e^{\chi_R(d-1)L/2} e^{-\lambda(L-x)} \right\}, \quad (\text{A11})$$

$$\frac{m_x^{(0)}}{n_c^{(0)}} = \frac{\lambda}{d(d-1)} \left\{ -e^{-\chi_R(d-1)L/2} e^{-\lambda x} + e^{\chi_R(d-1)L/2} e^{-\lambda(L-x)} \right\} \quad (\text{A12})$$

while the first order solution is

$$\begin{aligned} n^{(1)} = e^{-\chi_R(d-1)L/2} e^{-\lambda x} & \left\{ -\frac{\chi_R \text{Pe}^3 n_c^{(0)}}{2\lambda d^2} x \right. \\ & \left. + \frac{\text{Pe}}{d(d-1)} \left(n_c^{(1)} + \frac{\chi_R \lambda L d (d-1)^2 n_c^{(0)}}{2\text{Pe}} - \frac{\chi_R \text{Pe} n_c^{(0)}}{d} \right) \right\} \\ & + e^{\chi_R(d-1)(x-\frac{L}{2})} \left(n_c^{(1)} - \frac{\chi_R \lambda d (d-1)^2 n_c^{(0)}}{\text{Pe}} \left(x - \frac{L}{2} \right) \right) \\ & + e^{\chi_R(d-1)L/2} e^{-\lambda(L-x)} \left\{ \frac{\chi_R \text{Pe}^3 n_c^{(0)}}{2\lambda d^2} (L-x) \right. \\ & \left. + \frac{\text{Pe}}{d(d-1)} \left(n_c^{(1)} - \frac{\chi_R \lambda L d (d-1)^2 n_c^{(0)}}{2\text{Pe}} + \frac{\chi_R \text{Pe} n_c^{(0)}}{d} \right) \right\}, \quad (\text{A13}) \end{aligned}$$

$$\begin{aligned} m_x^{(1)} = e^{-\chi_R(d-1)L/2} e^{-\lambda x} & \left\{ \frac{\chi_R \text{Pe}^2 n_c^{(0)}}{2d^2 \lambda} (\lambda x - 1) \right. \\ & \left. - \frac{\lambda}{d(d-1)} \left(n_c^{(1)} + \frac{\chi_R \lambda L d (d-1)^2 n_c^{(0)}}{2\text{Pe}} - \frac{\chi_R \text{Pe} n_c^{(0)}}{d} \right) \right\} \\ & + \frac{\chi_R \lambda (d-1) n_c^{(0)}}{\text{Pe}} e^{\chi_R(d-1)(x-\frac{L}{2})} \\ & + e^{\chi_R(d-1)L/2} e^{-\lambda(L-x)} \left\{ \frac{\chi_R \text{Pe}^2 n_c^{(0)}}{2d^2 \lambda} (\lambda(L-x) - 1) \right. \\ & \left. + \frac{\lambda}{d(d-1)} \left(n_c^{(1)} - \frac{\chi_R \lambda L d (d-1)^2 n_c^{(0)}}{2\text{Pe}} + \frac{\chi_R \text{Pe} n_c^{(0)}}{d} \right) \right\}. \quad (\text{A14}) \end{aligned}$$

The concentration at the center of the confinement at leading and first order, $n_c^{(0)}$, $n_c^{(1)}$, respectively, can be found from the constraints $\frac{1}{L} \int_0^L n^{(0)} dx = \langle n \rangle$ and $\int_0^L n^{(1)} dx = 0$. In addition to the constraint $\chi_R \ll \text{Pe}$, we need also $\chi_R \leq O(1)$ for this theory to hold because otherwise the nematic order becomes large enough to invalidate the zero nematic order closure based on which this theory is built.

In the main text, we only considered the leading order solution to develop a simple theory. But the accuracy of this theory and hence the match with Brownian Dynamics (BD) simulations can be improved by considering the next order solution. For instance, the number density and polar order reported in Fig. 4 in the main text become those shown in Fig. 6 here, upon inclusion of the next order solution; the improvement in matching with the BD simulations is apparent.

If the orienting field is not constant and varies spatially, $\mathbf{H} = H(x) \hat{\mathbf{H}}$, then the asymptotic solution for field strengths $\chi_R \ll \lambda \sim \text{Pe}$ is

$$\frac{n}{n_c} = e^{-\chi_R(d-1)G(L/2)} \left\{ + \frac{\text{Pe}}{d(d-1)} \left(e^{\chi_R(d-1)G(0)} e^{-\lambda x} + e^{\chi_R(d-1)G(L)} e^{\lambda(x-L)} \right) \right\} + O\left(\text{Pe}^{-1}, \frac{\chi_R}{\text{Pe}}\right), \quad (\text{A15})$$

$$\frac{m_x}{n_c} = \frac{\lambda e^{-\chi_R(d-1)G(L/2)}}{d(d-1)} \left\{ -e^{\chi_R(d-1)G(0)} e^{-\lambda x} + e^{\chi_R(d-1)G(L)} e^{\lambda(x-L)} \right\} + O\left(\text{Pe}^{-1}, \frac{\chi_R}{\text{Pe}}\right). \quad (\text{A16})$$

Here, $G(x) = \int H(x) dx$ and the concentration at the center of the confinement n_c can again be found from the constraint $\frac{1}{L} \int_0^L n dx = \langle n \rangle$.

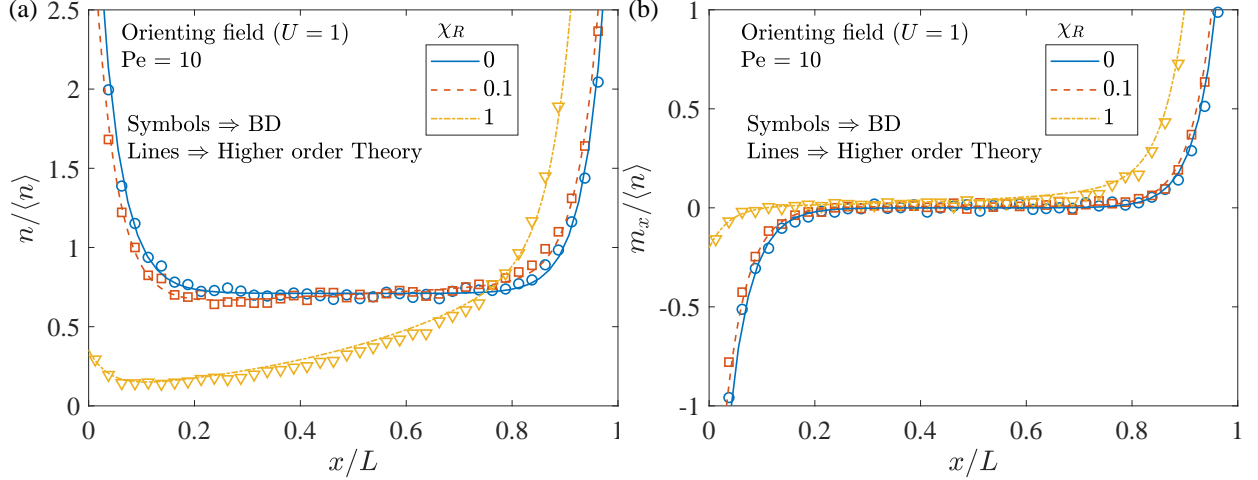


FIG. 6: The number density (a), and the polar order (b) associated with the active matter subjected to the orienting field. The symbols denote the BD simulation results while the lines represent the higher order theory. The confinement region L is 10 times larger than the microscopic length h .

Appendix B: Brownian Dynamics simulations

The Brownian Dynamics simulations reported in the main text are carried out by numerically integrating overdamped Langevin equations in time [34]

$$\mathbf{0} = -\zeta \dot{\mathbf{x}} + \mathbf{F}^{swim} + \mathbf{F}^B, \quad (\text{B1})$$

$$\mathbf{0} = -\zeta_R \dot{\boldsymbol{\Omega}} + \mathbf{L}^{ext} + \mathbf{L}^R, \quad (\text{B2})$$

where the particle orientation \mathbf{q} follows $\frac{d\mathbf{q}}{dt} = \boldsymbol{\Omega} \times \mathbf{q}$. Here ζ , ζ_R , are the translational and rotational resistances. The swim force $\mathbf{F}^{swim} = \zeta U(\mathbf{x}) \mathbf{q}$ and the torque exerted by the orienting field $\mathbf{L}^{ext} = \zeta_R \Omega_c (\mathbf{q} \times \mathbf{H})$. The fluctuating force \mathbf{F}^B and the torque \mathbf{L}^R follow the usual white noise statistics: $\overline{\mathbf{F}^B(t)} = \mathbf{0}$, $\overline{\mathbf{F}^B(0) \mathbf{F}^B(t)} = 2k_B T \zeta \delta(t) \mathbf{I}$, $\overline{\mathbf{L}^R(t)} = \mathbf{0}$, $\overline{\mathbf{L}^R(0) \mathbf{L}^R(t)} = 2\zeta_R^2 \delta(t) \mathbf{I} / \tau_R$, where the overbar denotes an ensemble average.

The numerical integration of the Langevin equations is carried out using the Euler-Maruyama scheme with the time-step $\Delta t = 10^{-4} \tau_R$ [35]. The simulations are run for 10^5 particles until the time $t = 100 \tau_R$. The penetration of particles into the wall is avoided by using the potential-free algorithm [36]. The wall separation L already includes the particle size, and thus the algorithm simplifies to setting the particle position x to 0 or L , respectively, if $x < 0$ or $x > L$.

Appendix C: Nematic order

We also solved the Smoluchowski equation numerically using in-house FEM code. The numerical solution yields the probability density, from which its moments were evaluated. The first two moments, the number density and the polar order, computed are consistent with theory and BD simulations. Typical values of the next moment, nematic order, at various Pe , χ_R and α_L are shown in Fig. 7. Nematic order is small and hence we assume it is safe to neglect for $Pe < 10^3$ and field strengths $\alpha_L < 1, \chi_R < 1$.

-
- [1] F. Schweitzer, *Browning agents and active particles* (Springer, Berlin, 2007).
 - [2] J. Toner, Y. Tu, and S. Ramaswamy, Hydrodynamics and phases of flocks, *Ann. Phys. (N.Y.)* **318**, 170 (2005).
 - [3] R. Alert, J. Casademunt, and J.-F. Joanny, Active turbulence, *Annu. Rev. Condens. Matter Phys.* **13**, 143 (2022).
 - [4] M. E. Cates and J. Tailleur, Motility-induced phase separation, *Annu. Rev. Condens. Matter Phys.* **6**, 219 (2015).

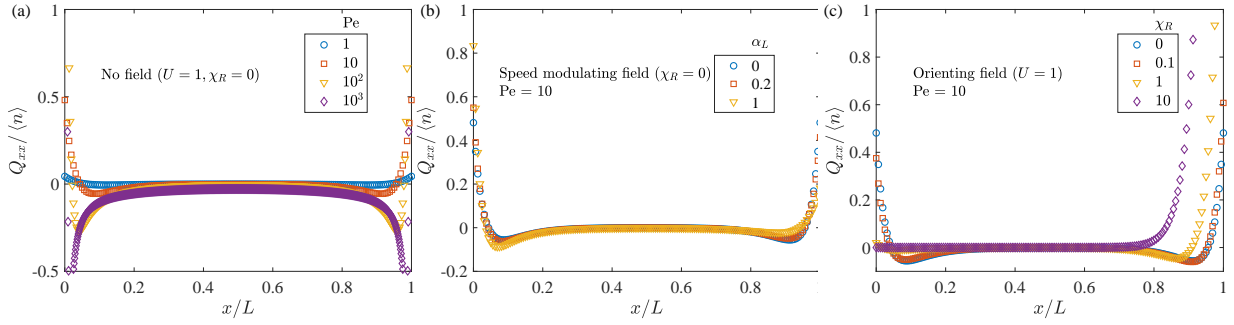


FIG. 7: The nematic order associated with the active matter without any field (a), or subjected to a speed modulating field (b) or an orienting field (c). The confinement region L is chosen as 10 times larger than the microscopic length h .

- [5] G. Volpe, I. Buttinoni, D. Vogt, H.-J. Kümmerer, and C. Bechinger, *Microswimmers in patterned environments*, *Soft Matter* **7**, 8810 (2011).
- [6] I. Buttinoni, G. Volpe, F. Kümmel, G. Volpe, and C. Bechinger, *Active Brownian motion tunable by light*, *J. Phys. Condens. Matter* **24**, 284129 (2012).
- [7] J. Palacci, S. Sacanna, A. P. Steinberg, D. J. Pine, and P. M. Chaikin, *Living crystals of light-activated colloidal surfers*, *Science* **339**, 936 (2013).
- [8] T. D. Ross, H. J. Lee, Z. Qu, R. A. Banks, R. Phillips, and M. Thomson, *Controlling organization and forces in active matter through optically defined boundaries*, *Nature (London)* **572**, 224 (2019).
- [9] R. Zhang, S. A. Redford, P. V. Ruijgrok, N. Kumar, A. Mozaffari, S. Zemsky, A. R. Dinner, V. Vitelli, Z. Bryant, M. L. Gardel, and J. J. de Pablo, *Spatiotemporal control of liquid crystal structure and dynamics through activity patterning*, *Nat. Mater.* **20**, 875 (2021).
- [10] S. C. Takatori and J. F. Brady, *Swim stress, motion, and deformation of active matter: effect of an external field*, *Soft Matter* **10**, 9433 (2014).
- [11] M. A. Fernandez-Rodriguez, F. Grillo, L. Alvarez, M. Rathlef, I. Buttinoni, G. Volpe, and L. Isa, *Feedback-controlled active Brownian colloids with space-dependent rotational dynamics*, *Nat. Commun.* **11**, 4223 (2020).
- [12] J. O. Kessler, *Hydrodynamic focusing of motile algal cells*, *Nature* **313**, 218 (1985).
- [13] J. Arlt, V. A. Martinez, A. Dawson, T. Pilizota, and W. C. K. Poon, *Painting with light-powered bacteria*, *Nat. Commun.* **9**, 768 (2018).
- [14] M. J. Schnitzer, *Theory of continuum random walks and application to chemotaxis*, *Phys. Rev. E* **48**, 2553 (1993).
- [15] J. Tailleur and M. E. Cates, *Statistical mechanics of interacting run-and-tumble bacteria*, *Phys. Rev. Lett.* **100**, 218103 (2008).
- [16] M. E. Cates and J. Tailleur, *When are active Brownian particles and run-and-tumble particles equivalent? Consequences for motility-induced phase separation*, *Europhys. Lett.* **101**, 20010 (2013).
- [17] J. Arlt, V. A. Martinez, A. Dawson, T. Pilizota, and W. C. K. Poon, *Dynamics-dependent density distribution in active suspensions*, *Nat. Commun.* **10**, 2321 (2019).
- [18] H. Row and J. F. Brady, *Reverse osmotic effect in active matter*, *Phys. Rev. E* **101**, 062604 (2020).
- [19] W. Yan and J. F. Brady, *The swim force as a body force*, *Soft Matter* **11**, 6235 (2015).
- [20] W. Yan and J. F. Brady, *The force on a boundary in active matter*, *J. Fluid Mech.* **785**, R1 (2015).
- [21] S. C. Takatori, W. Yan, and J. F. Brady, *Swim pressure: stress generation in active matter*, *Phys. Rev. Lett.* **113**, 028103 (2014).
- [22] W. Yan and J. F. Brady, *Anisotropic swim stress in active matter with nematic order*, *New J. Phys.* **20**, 053056 (2018).
- [23] M. R. Stehnach, N. Waisbord, D. M. Walkama, and J. S. Guasto, *Viscophobic turning dictates microalgae transport in viscosity gradients*, *Nat. Phys.* **17**, 926 (2021).
- [24] S. C. Takatori, R. De Dier, J. Vermant, and J. F. Brady, *Acoustic trapping of active matter*, *Nat. Commun.* **7**, 10694 (2016).
- [25] C. Datt and G. J. Elfring, *Active particles in viscosity gradients*, *Phys. Rev. Lett.* **123**, 158006 (2019).
- [26] V. A. Shaik and G. J. Elfring, *Hydrodynamics of active particles in viscosity gradients*, *Phys. Rev. Fluids* **6**, 103103 (2021).
- [27] C. Bechinger, R. Di Leonardo, H. Löwen, C. Reichhardt, G. Volpe, and G. Volpe, *Active particles in complex and crowded environments*, *Rev. Mod. Phys.* **88**, 045006 (2016).
- [28] D. Saintillan and M. J. Shelley, *Active suspensions and their nonlinear models*, *C. R. Phys.* **14**, 497 (2013).
- [29] S. Hess, *Tensors for Physics*, Undergraduate Lecture Notes in Physics (Springer International Publishing, Cham, 2015).
- [30] S. C. Takatori and J. F. Brady, *Towards a thermodynamics of active matter*, *Physical Review E* **91**, 032117 (2015).
- [31] D. Saintillan and M. J. Shelley, *Instabilities, pattern formation, and mixing in active suspensions*, *Phys. Fluids* **20**, 123304 (2008).
- [32] T. Gao, M. D. Betterton, A.-S. Jhang, and M. J. Shelley, *Analytical structure, dynamics, and coarse graining of a kinetic model of an active fluid*, *Phys. Rev. Fluids* **2**, 093302 (2017).

- [33] S. Weady, D. B. Stein, and M. J. Shelley, Thermodynamically consistent coarse-graining of polar active fluids, *Phys. Rev. Fluids* **7**, 063301 (2022).
- [34] M. D. Graham, *Microhydrodynamics, Brownian Motion, and Complex Fluids* (Cambridge University Press, Cambridge, England, 2018).
- [35] P. E. Kloeden and E. Platen, *Numerical Solution of Stochastic Differential Equations* (Springer, Berlin, 1992).
- [36] D. R. Foss and J. F. Brady, Brownian dynamics simulation of hard-sphere colloidal dispersions, *J. Rheol.* **44**, 629 (2000).